

HIGH MOLYBDENUM SILICON CAST IRON CRYSTALLIZATION PROCESS

STAWARZ Marcin¹, NUCKOWSKI Paweł Maciej², DOJKA Malwina¹

¹Silesian University of Technology, Faculty of Mechanical Engineering, Department of Foundry Engineering, Gliwice, Poland, EU, marcin.stawarz@polsl.pl

²Silesian University of Technology, Faculty of Mechanical Engineering, Institute of Engineering Materials and Biomaterials, Gliwice, Poland, EU

Abstract

The article presents results of studies of silicon - molybdenum cast iron crystallization process. This material is used to work in high temperatures. The study included experimental melting (estimated chemical composition was: 4.5 %Si; 2.5 %Mo; 2.5 %C) and analysis of crystallization process. For examination the TDA equipment was used for registration of temperature changes in time and for calculation of derivative curve. The analysis of chemical composition of obtained samples using spectrometer GDS500A and Leco analyser was conducted. Metallographic examination of cast alloys was carried out on Phenom Pro-X scanning microscope. In order to determine the phase composition, X-ray diffraction studies of analyzed samples were performed. These studies were carried on the Panalytical X'Pert PRO diffraction system, using filtered radiation from the lamp with copper anode and PIXcel 3D detector on the diffracted beam axis. Obtained results allowed to describe the crystallization process of ductile silicon - molybdenum cast iron (SiMo) designed to work in high temperatures. It was also possible to identify the elements of microstructure.

Keywords: Crystallization process, thermal derivative analysis, SiMo, silicon cast iron

1. INTRODUCTION

The most important advantages of cast iron containing from 4-6 % silicon and molybdenum is low price, good oxidation resistance, dimensional stability, high resistance to high operating temperatures, thermal shock and temperature cycling resistance [1-3]. For most applications, the Mo content in the range of 0.5 to 1 % provides the appropriate strength in elevated temperature and creep resistance. Higher additions of molybdenum are used, when it is necessary to maximize strength at higher temperature. High molybdenum addition, more than 1 % causes the formation of interdendritic type Mo₂C [4] carbides which are stable even after annealing and decrease the strength and ductility of the alloy in room temperature [5].

The content of molybdenum in SiMo cast iron defines the specific application of alloy:

- 0.0-0.5 % for applications with large and fast cycling temperatures,
- 0.5-1.0 % for applications with creep (long time in high temperature),
- 1.5-2.0 % for applications that require a high strength in high temperature (creep resistance or very high temperature) [5].

The main applications of SiMo cast iron are: exhaust manifolds for combustion engines, gas turbine components, moulds for casting of zinc, titanium and brass alloys, stands, holders for heat treatment (cyclic temperature changes), the elements of furnaces for heat treatment etc.

The material with nodular graphite has a stable ferrite structure (> 80 %), a small amount of molybdenum carbides (< 5 % for a molybdenum addition up to 2.5 %) and possibly some pearlite. When there is more than 6.5 % silicon present, several silicon products that cause brittleness, are formed (silicides).

In the temperature range between 600 °C and the Ac₁-temperature, generally pearlite, bainite and martensite will transform into ferrite and graphite. This transformation causes a loss of strength and an increase in volume, which mostly causes small cracks. Therefore the percentage of pearlite of the material in service must be

limited. If there is too much pearlite in the as cast condition, this must be corrected by a heat treatment. The higher the service temperature, the lower the maximum allowed pearlite content has to be. This is because pearlite will transform faster, with increasing temperature, into ferrite and graphite, which is not preferred [6].

The addition of silicon for SiMo cast iron should be between 4 and 6 %. The following rule can be noticed: the higher the silicon content, the greater is the resistance of the alloy to oxidation. Keep in mind that as the Si content increases, the tensile strength increases as well while the plasticity is decreasing. Too high Si content results in the formation of silicon compounds with iron [7] which increase the brittleness of the alloy. Molybdenum counteracts graphitization during eutectic crystallization, but significantly less than chromium. The eutectic carbide (Fe, Mo)₂₃C₆ appears, when the Mo content is over 1 % for ductile iron and for the cast iron with flake graphite over about 2 % of Mo. Due to the high Mo content, those carbides do not decompose even during long-term heat treatment, they can only be nodularized. Molybdenum is also present in the cast iron as a cementite and M₇C₃ and M₂C carbides [8].

An increasing molybdenum content will increase the pearlite content. Therefore it is preferred, for high molybdenum contents, to do a heat treatment [6].

Manganese promotes pearlite formation and therefore the level must be limited. The maximum value is 0.5 %. The disadvantage is that the presence of manganese sulfides decrease strength at higher temperatures.

2. RESEARCH DESCRIPTION AND RESULTS DISCUSSION

2.1. Methodology

Experimental melts were conducted in the induction furnace with medium frequency and the capacity of 25 kg [9-12]. The charge consisted of steel scrap with low sulphur content [13-14]. Other ingredients added during the melting was ferrosilicon FeSi75, Ranco carburizer and FeMo65 rich alloy. Magnesium rich alloy used in the studies was FeSiMg5RE. The spheroidization process of cast iron was conducted in the bottom of the ladle. The TDA analysis was conducted using Crystaldigraph NT-2T converter with the Electronite cup-shaped tester with shell mould that contained NiCr-Ni thermocouple (K-type) [10]. During melting the temperature of liquid metal in the furnace was controlled by immersion thermocouple (type S). Samples for chemical analysis were taken from the ladle after the spheroidization of cast iron. Metallographic examinations were carried out using SEM technology (Phenom Pro-X Scanning Electron Microscope with EDS). The analyzed microsections were etched with 5 % nital and not etched. Chemical composition analysis was performed on a Leco GDS500A spectrometer. Additionally, the content of carbon and sulfur was determined on the C and S Leco analyzer (CS125 Carbon-Sulfur Determinator). In order to determine the phase composition, X-ray diffraction studies of analyzed samples were performed. This studies were carried on the Panalytical X'Pert PRO diffraction system, using filtered radiation from the lamp with copper anode and PIXcel 3D detector on the diffracted beam axis [15]. Measurement was made by step method using cobalt K α radiation coupling continuous scanning in 2 θ range of 20-120° with current flow 1.7909 A, step space 0.026° and scanning time per step 100 s.

2.2. Chemical composition

The results of the chemical composition analysis for the analyzed melt were presented in **Table 1**. The results for C and S were corrected based on the results of C and S analysis with Leco Carbon-Sulfur Determinator CS125.

Table 1 Chemical composition of tested cast iron

*C (%)	Si (%)	Mo (%)	Mn (%)	P (%)	*S (%)	Mg (%)
2.48	4.42	2.59	0.83	0.022	0.0097	0.034
*Corrected result based on carbon and sulfur analysis on CS125 Carbon -Sulfur Determinator from Leco						

2.3. TDA analysis

Figure 1 shows a graph of temperature changes over time with the calculated first temperature derivative over time for the analyzed alloy. The thermal effect corresponding to the liquidus temperature is clearly seen. The liquidus temperature for tested alloy is 1188 °C. Another thermal effect from eutectic crystallization is visible for the time interval 111 and 163 s, in the temperature range 1111 °C and 1104 °C. At 1054 °C there is the maximum heat generated by the crystallization of the Mo₂C carbide phase. Between temperatures 1000 °C and 800 °C minor thermal effects are visible on the temperature derivative curve, which are caused by the crystallization of silicide phases, for example MnSi. In the range of temperatures between 796 °C - 695 °C the eutectoid transition was recorded.

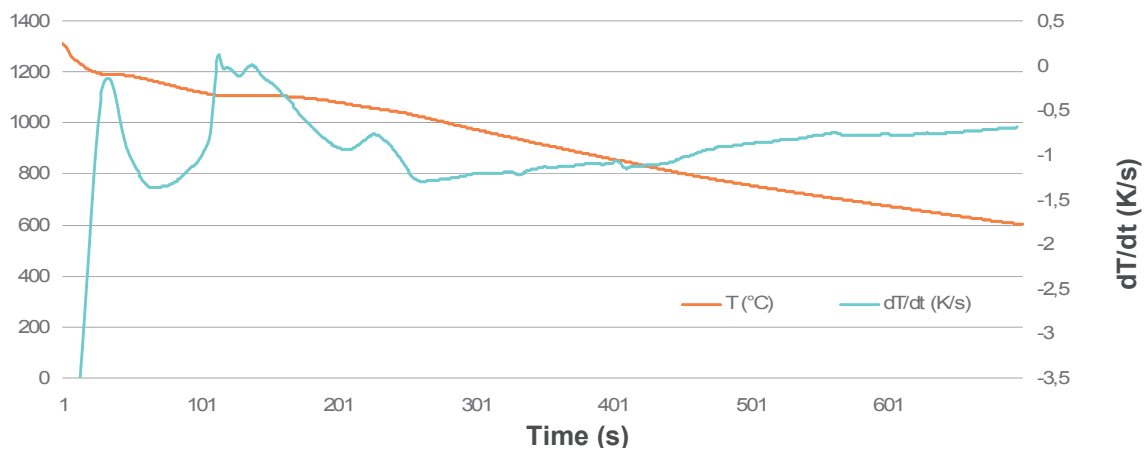


Figure 1 TDA curves for SiMo ductile iron

2.4. Metallographic analysis

The results of metallographic examinations were presented in **Figure 2**. Dark graphite precipitates can be clearly seen in the metal matrix consisted of light precipitates of carbide phase enriched with molybdenum (**Figure 2b**) and pearlite (dark areas). Lokaly, around the graphite precipitates the ferrite matrix was noticed. The degenerated graphite precipitates were also observed analyzed metallographic section which are visible in **Figure 2a**.

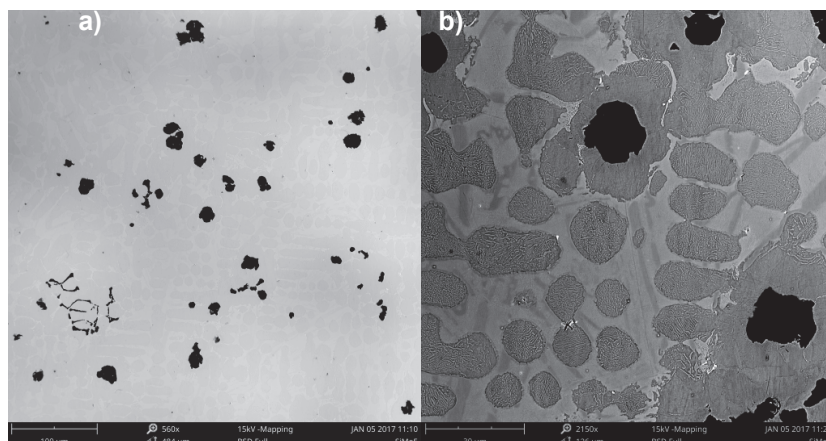


Figure 2 Microstructure of SiMo ductile iron, SEM

2.5. EDS analysis

Figure 3 shows the selected place of microstructure of experimental alloy, where the line scan was conducted. The results of linear EDS analysis for the examined areas of microsection were presented below.

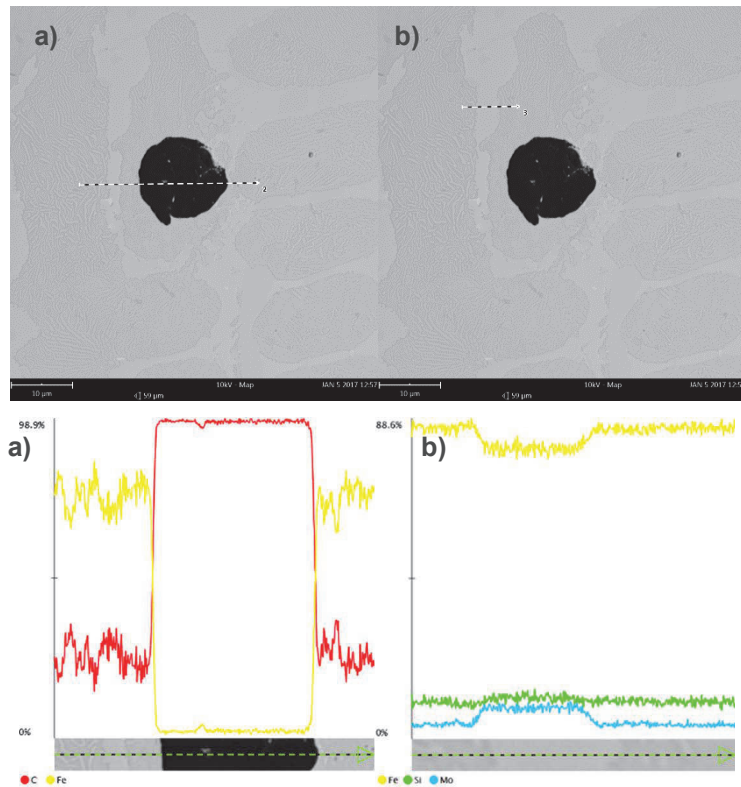


Figure 3 SiMo ductile iron EDS analysis. a) line scan of spheroidal graphite, b) line scan of molybdenum carbide phase

Figure 4 presents the map analysis of alloy matrix. The light molybdenum carbides and dark pearlite phase are visible in the metal matrix. Conducted map analysis of this place confirmed that the analyzed light areas in **Figure 4** are enriched with molybdenum (marked with blue). There can be also seen the Fe distribution (marked with yellow) and Si (marked with green).

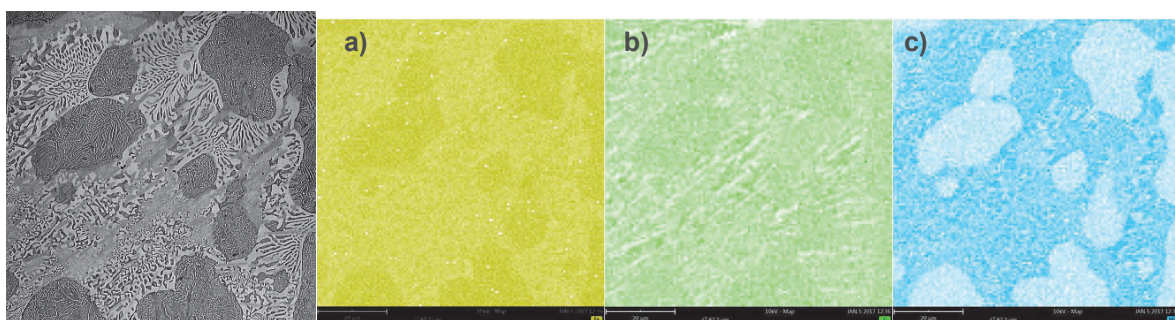


Figure 4 SiMo ductile iron EDS analysis. a) iron map, b) silicon map, c) molybdenum map

2.6. X-ray diffraction analysis

The X-ray diffraction allowed to identify phases forming the alloy. The results of this analysis were presented in **Figure 5**. The carbide phase with high amount of molybdenum were defined as Mo_2C molybdenum carbide. In analyzed alloy there is also cementite (Fe_3C) as the component of pearlite. The silicide phase is also present in the sample as MnSi silicide [16].

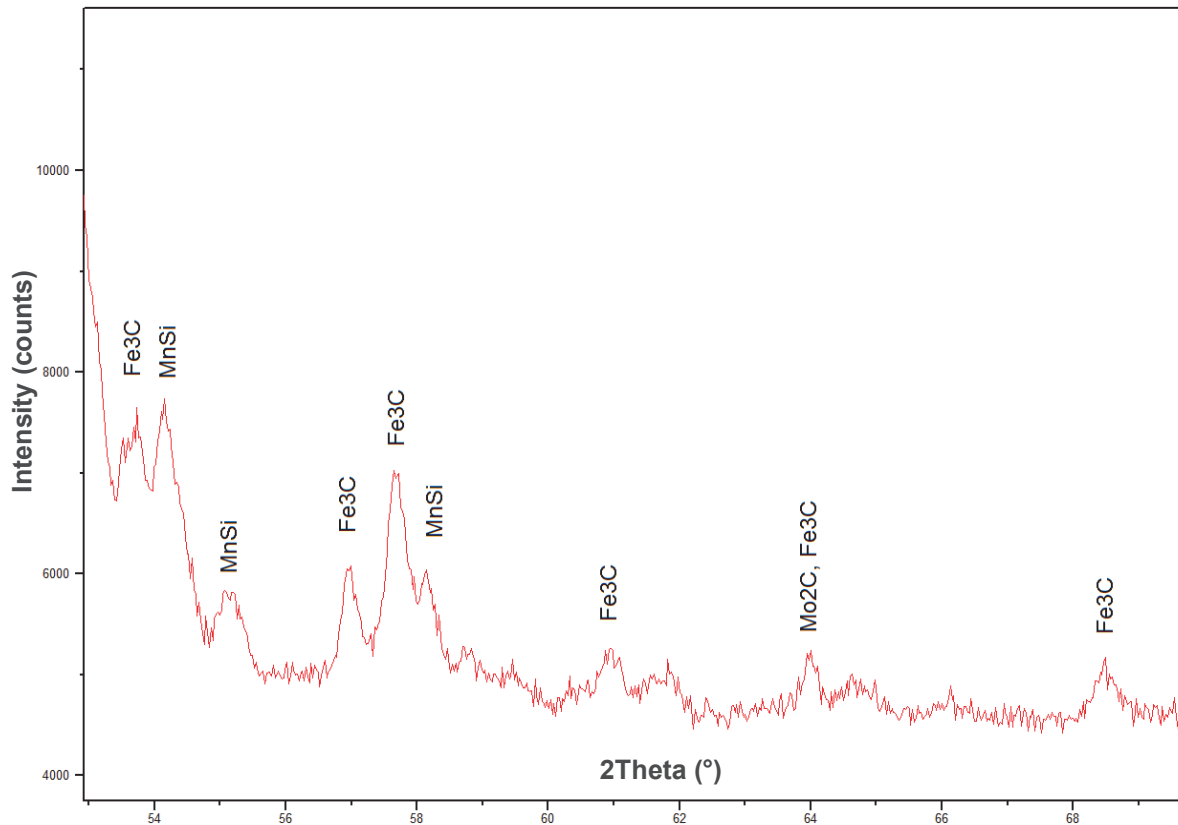


Figure 5 SiMo ductile iron X-ray diffraction analysis

3. CONCLUSION

The conducted studies allowed to record the characteristic temperatures of phase transitions [17] during the crystallization of tested alloy. The thermal effect corresponding to the liquidus temperature is clearly seen on TDA graph. The liquidus temperature for tested alloy is 1188 °C. Another thermal effect from eutectic crystallization is visible for the time interval 111 and 163 s, in the temperature range 1111 °C and 1104 °C. At 1054 °C there is the maximum heat generated by the crystallization of the Mo₂C carbide phase. Between temperatures 1000 °C and 800 °C minor thermal effects are visible on the temperature derivative curve, which are caused by the crystallization of silicide phases, for example MnSi. In the range of temperatures between 796 °C-695 °C the eutectoid transition was recorded. Basing on obtained results all the phases appearing in the alloy were identified. The analyzed SiMo cast iron microstructure consists of nodular graphite with a small amount of degenerated graphite with a distribution similar to interdendritic. Another component of microstructure is the molybdenum carbide (Mo₂C), clearly visible in the form of bright precipitates. There is also perlite and ferrite in the matrix of the tested cast iron. In this case, the presence of perlite in the alloy which will be working in high temperature conditions is harmful due to the possibility of small crack formation during cyclic temperature changes where the alloy should operate. Therefore, it is proposed to remove pearlite by applying heat treatment (ferritic annealing) and reduce the Mn content in the metal charge. In the analyzed case, silicide phase MnSi is also present in the cast iron matrix. Those phases decrease the tensile strength at high temperature conditions so therefore they should be eliminated by decreasing the Mn content in the charge material.

REFERENCES

- [1] DELPRETE, C., SESANA, R.,VERCELLI, A. Multiaxial damage assessment and life estimation: application to an automotive exhaust manifold. *Procedia Engineering* 2, 2010, pp. 725-734.

- [2] MATTEIS, P. SCAVINO, G., CASTELLO, A., FIRRAO, D. High temperature fatigue properties of a Si-Mo ductile cast iron. *Procedia Materials Science* 3, 2014, pp. 2154 - 2159.
- [3] GUZIK, E., WIERZCHOWSKI, D. Using cored wires injection 2PE-9 method in the production of ferritic Si-Mo ductile iron castings. *Archives of Foundry Engineering*, 2012, vol. 12, no. 4, pp. 53-56.
- [4] ABDERRAHIM, F.Z., FARAOUN, H.I., OUAHRANI, T. Structure, bonding and stability of semi-carbides M₂C and sub-carbides M₄C (M=V, Cr, Nb, Mo, Ta, W): A first principles investigation, *Physica B*, 2012, no. 407, pp. 3833-3838
- [5] ASM Handbook. Casting. 9th ed. Volume 15. ASM International, 1998. 1524 p.
- [6] HENDERIECKX, G.D. Silicon Cast Iron. Gietech BV, 2009. 44 p.
- [7] STAWARZ, M., GROMCZYK, M., JEZERSKI, J., JANERKA, K. Analysis of the high silicon cast iron crystallization process with TDA method. In *METAL 2015: 24th International Conference on Metallurgy and Materials*. Ostrava: TANGER 2015, pp. 42-47.
- [8] PODRZUCKI, C. Cast iron. Volume 1. Cracow: ZG STOP, 1991. 147-171 pp. (in polish)
- [9] TREPCZYŃSKA-ŁENT, M. Solid-liquid interface morphology of white carbide eutectic during directional solidification. *Archives of Metallurgy and Materials*, 2017, vol. 62, no. 1, pp. 365-368.
- [10] TREPCZYŃSKA-ŁENT, M., OLEJNIK, E. Solidification front of oriented ledeburite. *Archives of Foundry Engineering*, 2016, vol. 16, no. 1, pp. 124-130.
- [11] DULSKA, A., STUDNICKI, A., SZAJNAR, J. Reinforcing cast iron with composite insert. *Archives of Metallurgy and Materials*, 2017, vol. 62, no. 1, pp. 365-367.
- [12] SZAJNAR, J., DULSKA, A., WROBEL, T., BARON, C. Description of alloy layer formation on a cast steel substrate. *Archives of Metallurgy and Materials*, 2015, vol. 60, no. 3, pp. 2367-2372.
- [13] JANERKA, K., JEZERSKI, J., BARTOCHA, D., SZAJNAR, J. Analysis of ductile iron production on steel scrap base. *International Journal Of Cast Metals Research*, 2014, vol. 27, no. 4, pp. 230-234.
- [14] SZAJNAR, J., STAWARZ, M., WROBEL, T., SEBZDA, W. Influence of selected parameters of continuous casting in the electromagnetic field on the distribution of graphite and properties of grey cast iron. *Archives of Metallurgy and Materials*, 2014, vol. 59, no. 2, pp. 747-751.
- [15] NUCKOWSKI, P.M., KWAŚNY, W., RDZAWSKI, Z., GŁUCHOWSKI, W., PAWLYTA M. Influence of the Repetitive Corrugation on the Mechanism Occurring During Plastic Deformation of CuSn6 Alloy, *Archives of Metallurgy and Materials*, 2016, vol. 61, no 3, pp. 1261-1264.
- [16] BRINK-SHOEMAKER, C., SHOEMAKER, D.P. The Crystal Structure of the μ Phase, Mn_{81.5} Si_{18.5}. *Acta Crystallographica B*, 1971, vol. 27, pp. 227-235.
- [17] TREPCZYŃSKA-ŁENT, M. XRD and EBSD measurements of directional solidification Fe-C eutectic alloy. *Archives of Foundry Engineering*, 2016, vol. 16, no. 4, pp. 169-174.